Contents

Collective Behavior of Chiral Active Matter: Pattern Formation and Enhanced Flocking

Benno Liebchen[1,*] and Demian Levis[2,3,†]
[1]*SUPA, School of Physics and Astronomy, University of Edinburgh, Edinburgh EH9 3FD, United Kingdom*
[2]*Departament de Física de la Matèria Condensada, Universitat de Barcelona, Martí i Franquès 1, E08028 Barcelona, Spain*
[3]*Universitat de Barcelona Institute of Complex Systems (UBICS), Universitat de Barcelona, E08028 Barcelona, Spain*
(Received 20 January 2017; revised manuscript received 11 May 2017; published 1 August 2017)

We generalize the Vicsek model to describe the collective behavior of polar circle swimmers with local alignment interactions. While the phase transition leading to collective motion in 2D (flocking) occurs at the same interaction to noise ratio as for linear swimmers, as we show, circular motion enhances the polarization in the ordered phase (enhanced flocking) and induces secondary instabilities leading to structure formation. Slow rotations promote macroscopic droplets with late time sizes proportional to the system size (indicating phase separation) whereas fast rotations generate patterns consisting of phase synchronized microflocks with a controllable characteristic size proportional to the average single-particle swimming radius. Our results defy the viewpoint that monofrequent rotations form a vapid extension of the Vicsek model and establish a generic route to pattern formation in chiral active matter with possible applications for understanding and designing rotating microflocks.

DOI: 10.1103/PhysRevLett.119.058002

$$\dot{\mathbf{r}}_i = v \begin{bmatrix} \cos\theta_i \\ \sin\theta_i \end{bmatrix}$$

$$\dot{\theta} = \omega + \frac{K}{\pi R_\theta^2} \sum_{j \in \partial_i} \sin\left(\theta_j - \theta_i\right) + \sqrt{2D_r}\eta_i$$

$\eta_i(t)$ is a unit-variance Gaussian white noise with zero mean.

To reduce the parameter space to model's essential dimensions, the authors choose space and time units as R_θ and D_r^{-1}. Four dimensionless control parameters:

- $\rho_0 = NR_\theta^2/L^2$, the particle density
- $\mathrm{Re}_r = v/\left(D_r R_\theta\right)$, the Péclet number, measuring the persistence length in units of the alignment interaction range
- $g = K/\left(\pi R_\theta^2 D_r\right)$, the alignment strength
- $\Omega = \omega/D_r$, comparing alignment and rotational frequencies with the rotational diffusion rate

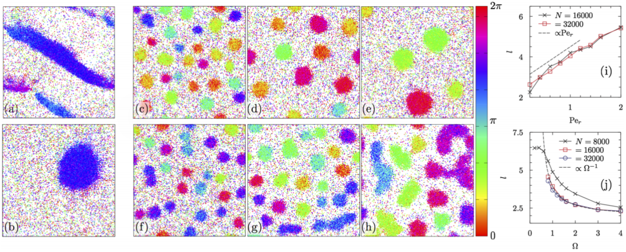

FIG. 2. Simulation snapshots for $N = 32\,000$ particles with colors encoding particle orientations. [(a), $\Omega = 0$]: Traveling bands; [(b), $\Omega = 0.2 < 1$]: rotating macrodroplet (phase separation) (c)–(h): Microflock pattern at $g\rho_0 = 2.8$, $\Omega = 3$, and $\mathrm{Pe}_r = 0.2$ (c), $\mathrm{Pe}_r = 1.0$ (d), and $\mathrm{Pe}_r = 2$ (e), and at $\mathrm{Pe}_r = 0.2$, $\Omega = 3$, and $g\rho_0 = 2.4$ (f), 3.6 (g), and 6 (h). (i), (j): Microflock length scale l for $g\rho_0 = 2.8$; for $\Omega = 3$ as a function of Pe_r (i), and for $\mathrm{Pe}_r = 0.2$ as a function of Ω (j) for the system sizes shown in the key.

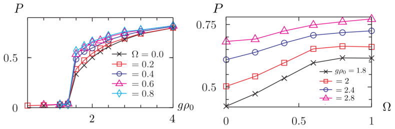

FIG. 3. Global polarization over $g\rho_0$ and Ω showing invariance of the flocking transition against rotations (left) and enhanced flocking (right) as predicted in the text.

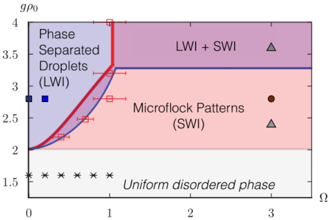

Contents

Pulsating Active Matter

Yiwei Zhang and Étienne Fodor
Department of Physics and Materials Science, University of Luxembourg, L-1511 Luxembourg, Luxembourg

(Received 13 December 2022; revised 18 July 2023; accepted 13 November 2023; published 8 December 2023)

We reveal that the mechanical pulsation of locally synchronized particles is a generic route to propagate deformation waves. We consider a model of dense repulsive particles whose activity drives periodic change in size of each individual. The dynamics is inspired by biological tissues where cells consume fuel to sustain active deformation. We show that the competition between repulsion and synchronization triggers an instability which promotes a wealth of dynamical patterns, ranging from spiral waves to defect turbulence. We identify the mechanisms underlying the emergence of patterns, and characterize the corresponding transitions. By coarse-graining the dynamics, we propose a hydrodynamic description of an assembly of pulsating particles, and discuss an analogy with reaction-diffusion systems.

DOI: 10.1103/PhysRevLett.131.238302

$$\dot{\mathrm{r}}_i = -\mu \sum_j \partial_{\mathrm{r}_i} U\left(a_{ij}\right) + \sqrt{2D}\xi_i$$

$$\dot{\theta}_i = \omega - \sum_j \left[\tau\left(a_{ij}, \theta_i - \theta_j\right) + \mu_\theta \partial_{\theta_i} U\left(a_{ij}\right)\right] + \sqrt{2D_\theta}\eta_i$$

$$\varphi = \pi \sum_{i=1}^{N} \left[\sigma\left(\theta_i\right)/L\right]^2$$

$$r = \frac{1}{N}\left|\sum_{j=1}^{N} e^{\mathrm{i}\theta_j}\right|$$

$$a_{ij} = \frac{\left|\mathrm{r}_i - \mathrm{r}_j\right|}{\sigma\left(\theta_i\right) + \sigma\left(\theta_j\right)}$$

$$\sigma\left(\theta_i\right) = \sigma_0 \frac{1 + \lambda \sin\theta_i}{1 + \lambda}$$

$$U(a) = \begin{cases} U_0\left(a^{-12} - 2a^{-6}\right), & a < 1 \\ 0, & \text{otherwise} \end{cases}$$

$$\tau(a, \theta) = \begin{cases} \varepsilon \sin(\theta), & a < 1 \\ 0, & \text{otherwise} \end{cases}$$

Symbols	Meanings
r	position
θ	phase, determining the particle size
U	pairwise repulsive potential
μ	self-propulsion mobility
D	diffusivity
ξ	isotropic Gaussian white noise
$\sigma(\theta)$	particle size
σ_0	largest size
$\lambda < 1$	pulsation amplitude

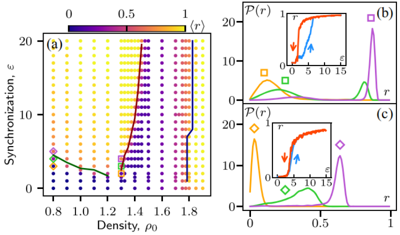

FIG. 2. Phases and transitions in particle-based dynamics. (a) We distinguish two ordered states ($\langle r \rangle \approx 1$) where particles are either cycling in phase (small ρ_0 and large ε) or arrested (large ρ_0). The solid lines in dark green [$\varepsilon_{b,1}(\rho_0)$], dark red [$\varepsilon_{b,2}(\rho_0)$], and dark blue [$\varepsilon_{b,3}(\rho_0)$] are guidelines delineating the boundaries between ordered and disordered states [39]. Dynamical patterns and waves (Fig. 1) emerge in the disordered state at large ε, in between the phase boundaries $\varepsilon_{b,2}(\rho_0)$ and $\varepsilon_{b,3}(\rho_0)$. (b) At $\rho_0 = 1.3$, the distribution $\mathcal{P}(r)$ changes between unimodal and bimodal shapes when varying ε through the phase boundary $\varepsilon_{b,2}(\rho_0)$ [squares in (a)]. The transition is discontinuous with hysteresis (inset). (c) At $\rho_0 = 0.8$, $\mathcal{P}(r)$ stays unimodal through the boundary $\varepsilon_{b,1}(\rho_0)$ [diamonds in (a)]. The transition is continuous without hysteresis (inset).

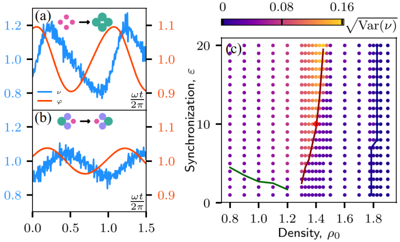

FIG. 3. Packing fraction φ and current ν oscillate in quadrature, with higher amplitude for (a) globally synchronized particles than for (b) dynamical patterns. Trajectories in (a) and (b) are sampled at the same point ($\varepsilon = 10, \rho_0 = 1.4$) of the phase diagram [red diamond in (c)]. (c) The current variance $\mathrm{Var}(\nu)$ changes abruptly close to the phase boundary $\varepsilon_{b,2}(\rho_0)$ [same line as in Fig. 2(a)].

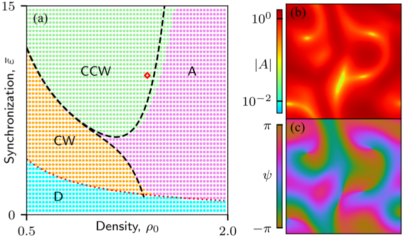

FIG. 4. (a) Phase diagram of homogeneous states in noiseless hydrodynamics: (D) disorder, (A) arrest, (CW) clockwise, and (CCW) counterclockwise cycles. The red dotted line delineates order-disorder transition. The black dashed lines approximate the stability of arrest [39]. (b),(c) In the presence of noise, steady states with motile defects appear for $(\bar{\varepsilon}, \rho_0)$ between cycling and arrest [diamond in (a)].

$$\partial_t A = \left(\frac{\bar{\varepsilon}\rho_0}{2} - D_\theta + \mathrm{i}\omega + D\nabla^2 \right) A - \frac{\bar{\varepsilon}^2 A\,|A|^2}{4\,(2D\theta - \mathrm{i}\omega)}$$
$$- \mathrm{i}cA \left[\mathrm{Re}\,(A) + \frac{\bar{\varepsilon}\lambda}{4} \mathrm{Im} \left(\frac{A^2}{2D\theta - \mathrm{i}\omega} \right) \right] + \sqrt{\rho_0 D_\theta}\Lambda$$